Sustainable Energy & Fuels

Electrochemically promoted ammonia synthesis on an Fe/BaZr0.8Y0.2O3-δ catalyst at ambient pressure

Journal:	*Sustainable Energy & Fuels*
Manuscript ID	SE-ART-10-2021-001712.R1
Article Type:	Paper
Date Submitted by the Author:	08-Dec-2021
Complete List of Authors:	Yuan, Yao; The University of Tokyo Tada, Shohei; Ibaraki University, Department of Materials Science and Engineering Kikuchi, Ryuji; The University of Tokyo, Department of Chemical System Engineering

ARTICLE

Electrochemically promoted ammonia synthesis on an $Fe/BaZr_{0.8}Y_{0.2}O_{3-\delta}$ catalyst at ambient pressure

Received 00th January 20xx,
Accepted 00th January 20xx

DOI: 10.1039/x0xx00000x

Yao Yuan,[a] Shohei Tada[b] and Ryuji Kikuchi*[a]

Electrochemically promoted nitrogen reduction on solid-state electrolytes is a promising approach for synthesising ammonia (NH_3) under mild conditions. In this study, yttrium-doped barium zirconate (BZY) was chosen as a solid-state electrolyte owing to its high chemical stability and NH_3 production on an Fe/BZY catalyst was investigated under open-circuit conditions and polarised conditions in a N_2–H_2 gas mixture at 500 °C and ambient pressure. NH_3 production was enhanced under applied voltages, and the highest production rate of 3.07×10^{-9} mol/(s cm^2) was achieved under polarised conditions. The reaction rates were observed to change gradually as the reaction progressed, both in the open-circuit state and under applied voltages. This slow response of the NH_3 production rate was modelled, and the electrochemical promotion of NH_3 production was explained by the gradual removal of H adatoms from the catalyst and the resultant increase in N adsorption sites. The modelling result indicated that a higher ratio of adsorbed nitrogen atoms (N*) to adsorbed hydrogen atoms (Hs) contributed to accelerating the NH_3 production rate.

Introduction

Ammonia (NH_3) is indispensable as a feedstock for fertilizers and chemical products. It has a worldwide annual production of up to 150 million tons,[1] which accounts for 1%–3% of global primary energy consumption.[2] In addition to its utility as a raw material, NH_3 is regarded as a potential hydrogen carrier and energy storage material[3] for renewable energy resources, and has been demonstrated as a fuel derived from energy resources for combustion[4] and fuel cells.[5]

Currently, NH_3 is mainly produced via the Haber–Bosch process, which uses N_2 separated from air and H_2 obtained by reforming fossil fuels such as natural gas and coal. The conventional Haber–Bosch process uses an Fe-based catalyst to produce NH_3 and remains one of the most important heterogeneous catalytic reactions. The Fe-based catalyst used in the Haber–Bosch process is fabricated using K_2O, Al_2O_3, and CaO-promoted magnetite (Fe_3O_4). The fused Fe_3O_4 is granulated mechanically and then reduced in syngas (a mixture of CO and H_2) to form the α-Fe catalyst.[6] Conventional Haber–Bosch processes are typically operated at elevated temperatures (400–500 °C) and pressures (15–20 MPa). However, the use of such high temperatures and pressures requires continuous NH_3 production at a rate of at least 600 tons of NH_3 per day to achieve economic competitiveness with other NH_3 production processes.[2]

Therefore, electrochemical nitrogen reduction processes that can be operated under mild conditions using renewable electricity have attracted considerable attention.[7] One of the most promising methods is an electrochemical process using solid-state electrolytes. Solid-state electrolytic cells require dense electrolytes with high proton conductivity, porous electrodes with high electronic conductivity and excellent stability under the operating condition, and a highly active catalyst.[8] Proton-conducting perovskite-type oxides such as Y-doped $SrZrO_3$ (SZY),[9] Y-doped $SrCeO_3$ (SCY),[10] and Y-doped $BaCeO_3$ (BCY)[11] have been reported as electrolytes for electrolytic NH_3 synthesis at approximately 500 °C and ambient pressure. A reaction rate of 2.36×10^{-9} mol/(s cm^2)[12] and a Faradaic efficiency of 60%[5] were achieved using a BCY electrolyte and Ag–Pd cathode catalysts to produce NH_3 from N_2 and H_2. However, to the best of our knowledge, electrolytic NH_3 synthesis using a BZY electrolyte has not been reported, except from steam and N_2 using Ag, Pt, and $La_{0.6}Sr_{0.4}Co_{0.2}Fe_{0.8}O_{3-\delta}$ (LSCF) cathode materials.[13] In a previous study on two-chamber electrochemical NH_3 synthesis using a Pt anode, a BCY electrolyte, and an Fe-BCY cathode modified with K and Al, it was reported that the NH_3 production rate was accelerated by cathode polarisation.[14] Vasileiou *et al*. also investigated the electrochemical enhancement of NH_3 production in a Ni-BZCY cell, and transient behaviour was observed.[15] However, the transient behaviour of Fe-based cathodes has not been reported, and the mechanistic origin of the promoting effect has not yet been determined.

[a] *Department of Chemical System Engineering, The University of Tokyo, 7-3-1, Hongo, Bunkyo-ku, Tokyo 113-8656, Japan. E-mail: rkikuchi@chemsys.t.u-tokyo.ac.jp*
[b] *Department of Materials Sciences and Engineering, Ibaraki University, Ibaraki 316-8511, Japan*
Electronic Supplementary Information (ESI) available: See
DOI: 10.1039/x0xx00000x

In this study, BZY was used as an electrolyte because it has greater chemical stability than BCY.[16] An Fe/BZY catalyst was fabricated from sintered Fe_2O_3/BZY and used as a cathode material for electrolytic NH_3 synthesis. Catalytic and electrolytic NH_3 synthesis processes were carried out in Fe/BZY-Pt|BZY|Pt cells in a single-chamber reactor using a H_2–N_2 mixture at 500 °C and ambient pressure. The gradual increase in the NH_3 production rate at applied voltages was modelled, and the intermediate species adsorbed on the cathode were analysed to obtain insights into the electrochemical promotion of the NH_3 production rate under polarised conditions.

Experimental

Preparation of a BZY pellet as an electrolyte[17]

Yttrium-doped barium zirconate ($BaZr_{0.8}Y_{0.2}O_{3-\delta}$) powders were prepared using a conventional solid-state reaction method. [18] $BaCO_3$ (98% purity, Wako Pure Chemical Industries Ltd.), Y_2O_3 (99.9% purity, Wako Pure Chemical Industries Ltd.), and ZrO_2 (98% purity, Wako Pure Chemical Industries Ltd.) were mixed in stoichiometric quantities by ball-milling in ethanol overnight. The mixture was heated to dryness and then calcined at 1400 °C for 12 h to form a BZY powder.

As a sintering aid, 1 wt% NiO (99.0+% purity, Wako Pure Chemical Industries Ltd.) was added to the BZY powder. The mixture was ball-milled and then pressed at 20 MPa for 10 min to form a Φ20 mm pellet. Subsequently, the pellet was subjected to cold isostatic pressing at 200 MPa for 15 min. Finally, sintering at 1400 °C for 12 h produced a Φ15 mm, 1 mm thick pellet.

Preparation of an α-Fe_2O_3/BZY[19] disk as a cathode catalyst

The BZY powder was mixed with α-Fe_2O_3 (20–40 nm, Wako Pure Chemical Industries Ltd.) in a ratio of 1:4 (w/w) by ball-milling in ethanol overnight. The precursor was heated to dryness and sintered at 1300 °C for 12 h to form an Fe_2O_3/BZY composite. Then, 0.6 g of Fe_2O_3/BZY was pressed at 20 MPa for 10 min to form a Φ10 mm disk. After calcination at 1300 °C for 5 h, a Φ10 mm, 2 mm thick disk was formed.

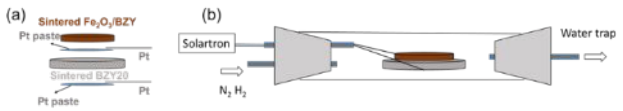

Fig. 1 (a) Preparation of the cell for electrocatalytic NH_3 synthesis. (b) Experimental setup.

Preparation of cells and experimental setup

A schematic of the cell for electrocatalytic NH_3 synthesis is shown in Fig. 1a. The Fe_2O_3/BZY electrode and the BZY were bound together by using Pt paste, which is relatively inactive for NH_3 synthesis. Sintering of the Fe_2O_3/BZY pellet and the BZY electrolyte was not feasible by high-temperature calcination owing to the diffusion of Fe into the BZY electrolyte during the sintering process. Therefore, the as-calcined Fe_2O_3/BZY disk was attached to the BZY pellet using Pt paste. Pt paste was also used as the anode catalyst for H_2 dissociation. Pt wires connected to the Pt paste on both sides were used as terminals. Finally, the cell was heat-treated at 900 °C for 2 h.

The cell was placed in a quartz glass tube with a 17 mm diameter as a simple single-chamber reactor (Fig. 1b). Experiments were carried out in a gas mixture of N_2 and H_2 (1:1, v/v) with a total gas flow rate of 50 mL/min at ambient pressure and 500 °C. The outlet gas was trapped using distilled water for 30 min. NH_3 was quantified by colorimetry (DR900, Hach Company) using the salicylate method (Nitrogen-Ammonia Reagent Set, Salicylate Method, 10 mL, Hach Company). A hydrazine reagent (HydraVer® 2 Hydrazine Reagent, Hach Company) was used for hydrazine quantification.

Control experiments under open-circuit conditions

Ambient NH_3 in air, the nitrogen-containing precursors of the catalyst, and the catalyst itself are potential sources of contaminant NH_3.[20,21] Therefore, to ensure accurate and reliable quantification of NH_3 produced during catalytic and electrocatalytic reactions, three control experiments were carried out. Control experiment 1 was carried out at 500 °C in dry Ar gas flow (50 mL/min) at the open-circuit voltage (OCV). Control experiment 2 was carried out at 500 °C in dry N_2 gas flow (25 mL/min) at the OCV. Control experiment 3 was carried out at 500 °C in dry H_2 gas flow (25 mL/min) at the OCV and an applied voltage of -0.6 V. The outlet gas was trapped using distilled water for 30 min and then analysed. The collection time was longer than or equal to that in the following catalytic and electrolytic experiments.

The amount of NH_3 trapped during the control experiments was below the detection limit (0.01 mg-N/L, equivalent to 2.5×10^{-11} mol/(s cm^2) during a collection period of 30 min). Therefore, the effect of ambient NH_3 could be ignored. Furthermore, no N_2H_4 was detected in the control experiments (detection limit of 1 μg-N_2H_4/L, equivalent to 1.1×10^{-12} mol/(s cm^2) during a collection period of 30 min). As the reagents used to synthesise the catalyst and electrolyte did not contain any N, these results confirmed that N in the produced NH_3 originated from N_2 gas in the feed.

Evaluation of catalytic activity for thermochemical and electrochemical reactions

The cell was pretreated at 500 °C for 1 h in H_2 gas flow (50 mL/min) before the NH_3 synthesis tests. Subsequently, the gas flow was changed to a mixture of N_2 (25 mL/min) and H_2 (25 mL/min). To distinguish NH_3 produced thermochemically or/and electrochemically from the total reaction rate, NH_3 synthesis experiments were carried out at the OCV using the as-prepared cell. The outlet gas was trapped using distilled water at intervals of 10 min until the reaction rate became constant.

During electrolytic operation for NH_3 synthesis, a direct current voltage versus OCV was applied between the anode and cathode in potentiostatic mode. The outlet gas was trapped using distilled water for 30 min. The alternating current impedance was measured for the cells under OCV conditions (Fig. S1), and the impedance data were fitted using an equivalent circuit (Fig. S2). The fitting results are shown in Fig. S3 and Table S1.

Characterisation of prepared materials

X-ray diffraction (XRD) patterns were collected in the 2θ range of 20°–80° using an X-ray diffractometer (Rigaku RINT 2400) operated at 100 kV and 40 mA. A sample cross-section was obtained by mechanical cracking and the morphology was observed by scanning electron microscopy (SEM; Hitachi S-900). The elemental composition was analysed using energy-dispersive X-ray spectroscopy (EDX; Super Xerophy, Horiba).

Results and discussion

Characterisation of prepared materials

The XRD pattern of Fe_2O_3/BZY after sintering at 1300 °C for 12 h revealed that some α-Fe_2O_3 was transformed into ε-Fe_2O_3 and γ-Fe_2O_3 (Fig. 2).[22] Furthermore, peaks corresponding to $BaCO_3$ were observed, which implied that BZY was partially decomposed during sintering. Added BZY could act as a proton conductor and barium could act as a promotor for NH_3 synthesis.[23] The XRD pattern of spent Fe/BZY revealed that Fe_2O_3 was reduced to Fe. The intensity of the perovskite peaks decreased and that of the $BaCO_3$ peaks increased after the electrocatalytic reaction, suggesting that BZY decomposition occurred during the electrocatalytic reaction. Peaks corresponding to γ-Fe were also observed in the XRD pattern of spent Fe/BZY, which were much weaker than those of α-Fe.

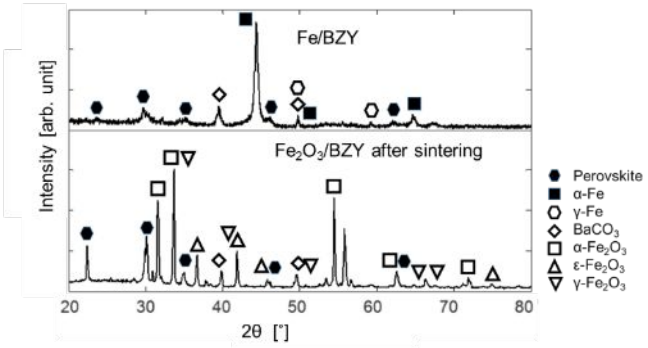

Fig. 2 XRD patterns of Fe_2O_3/BZY after sintering at 1300 °C for 12 h and spent Fe/BZY.

The cross-sectional SEM image of sintered Fe_2O_3/BZY revealed a dense structure (Fig. 3). After the electrocatalytic reaction, spent Fe/BZY became porous, and different morphologies such as blocks, layers, and particulates were observed (Fig. 4a, b, and d). Interestingly, several hexagons with diameters of less than 2 μm were distributed on the surfaces of the blocks (Fig. 4c and e). These hexagons were inferred to be

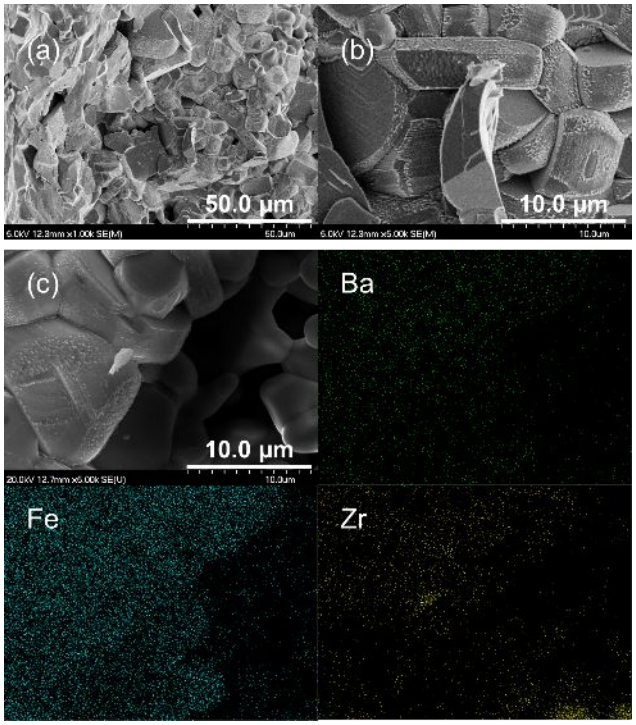

Fig. 3 (a,b) Cross-sectional SEM images and (c) EDX elemental mapping (Fe, Ba, and Zr) of Fe_2O_3/BZY (1:4, w/w) after sintering at 1300 °C for 12 h.

γ-Fe, which has an fcc phase and based on thermodynamics is expected to exist at high temperatures and low pressures.[24] Both γ-Fe and α-Fe have bcc phases that coexist at approximately 600 °C.[25] Thus, the applied voltage might have caused a phase transformation from α-Fe to γ-Fe in Fe/BZY at 500 °C and ambient pressure. As the solubility of N in γ-Fe is

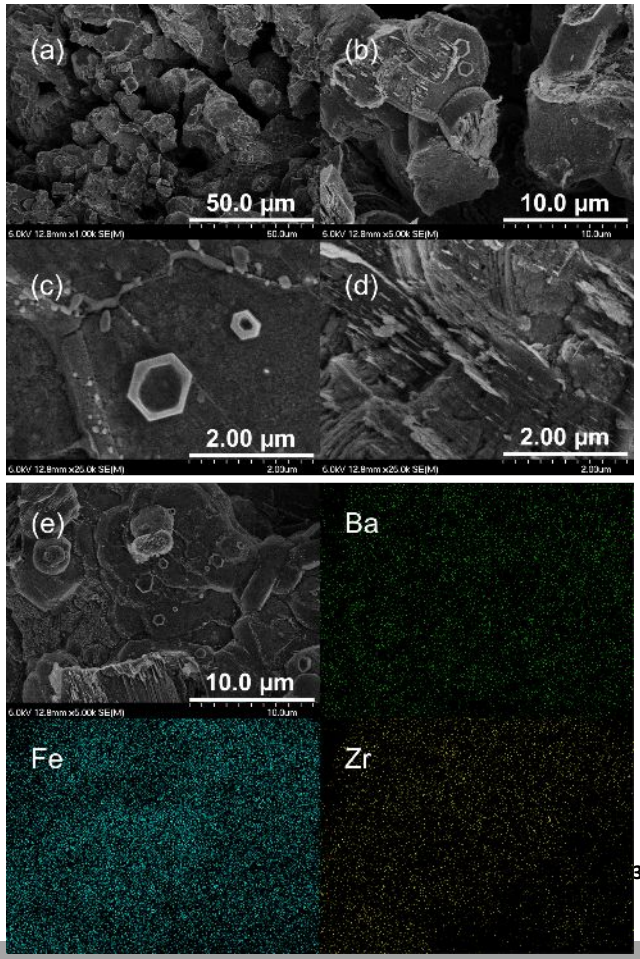

Fig. 4 (a–d) Cross-sectional SEM images and (e) EDX elemental mapping (Fe, Ba, and Zr) of spent Fe/BZY.

higher than that in α-Fe at 0.1 MPa,[25] γ-Fe could be favourable for NH_3 production.

Evaluation of catalytic activity and reaction rates under applied voltages

The catalytic activities and reaction rates for NH_3 synthesis were compared for catalytic and electrochemical reactions. As shown in Fig. 5, the NH_3 production rate gradually increased with time on stream not only at the OCV but also under applied voltages. A similar slow catalytic response was reported for the high-pressure electrochemical promotion of NH_3 synthesis

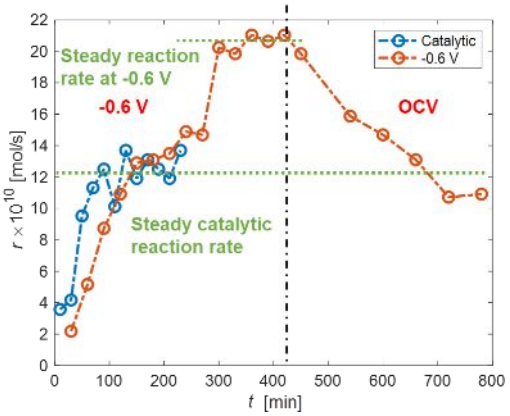

Fig. 5 Comparison of catalytic reaction rates (blue line) and electrocatalytic reaction rates (red line). In the electrocatalytic reaction, -0.6 V was applied from 0 to 450 min, whereas from 450 to 1020 min, the reaction was carried out at the OCV.

using an industrial Fe-based catalyst, which was ascribed to a long residence time of approximately 150 min.[26] However, in the current study, the single-chamber reactor consisted of a simple tube with a length of 40 cm and an inner diameter of 17 mm, for which the residence time was estimated to be approximately 0.55 min. Therefore, the residence time cannot be the reason for the slow response of the NH_3 production rate. Following the reduction of Fe_2O_3/BZY in flowing H_2 gas, the N_2 gas flow was introduced at the same time as trapping of the outlet gas was initiated. Therefore, it is assumed that the catalyst surface was initially covered with H adatoms. Then, the adsorbed H atoms were gradually released in the mixed gas flow. Thus, the number of unoccupied active sites for N_2 activation increased, leading to an enhancement of the production rate.

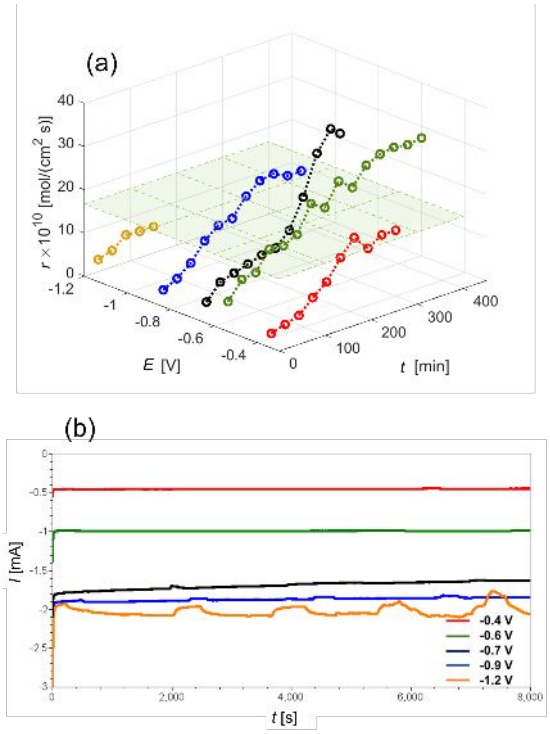

Fig. 6 (a) Reaction rates under applied voltages of -0.4 V (red), -0.6 V (blue), -0.7 V (black), -0.9 V (green), and -1.2 V (orange). The light green mesh plane shows the steady catalytic reaction rate. **(b)** Currents at applied voltages of -0.4, -0.6, -0.7, -0.9, and -1.2 V.

The NH_3 production rate at the OCV stabilised at 1.61×10^{-9} mol/(s cm^2) (equivalent to 2.10×10^{-9} mol/(g-cat s)) after more than 100 min. When a constant potential (-0.6 V) was applied from 0 to 450 min, the reaction rate was higher than that for the thermal catalytic reaction under the same conditions, eventually reaching a value of 2.71×10^{-9} mol/(cm^2 s). Constant polarisation at -0.6 V produced a constant current (I) of -1.0 mA, which supplied protons to the Fe/BZY catalyst at a rate of $-I/F = 1.0 \times 10^{-8}$ mol/s. Thus, the enhancement factor (defined as $\Lambda = (r - r\text{-cat}) \times 3/(-I/F)$, where r-cat is the steady catalytic production rate at the OCV and F is the Faraday constant) was 25.1%. At 450 min, the applied voltage of -0.6 V was switched to the OCV, which resulted in a gradual decrease of the reaction rate to 1.41 mol/(s cm^2) (equivalent to 1.85×10^{-9} mol/(g-cat s)), which was similar to the steady production rate for the thermal catalytic reaction. The gradual decrease of the reaction rate after switching to the OCV is typical transient behaviour, which has been commonly reported in studies on the non-Faradaic electrochemical modification of catalytic activity (NEMCA) effect.[27] If the reaction rate change was due to electrochemical effects, the reaction rate would be expected to decrease immediately upon switching to the OCV. Therefore, the observed behaviour indicates that the production rate enhancement is not an electrocatalytic phenomenon but a catalytic one.

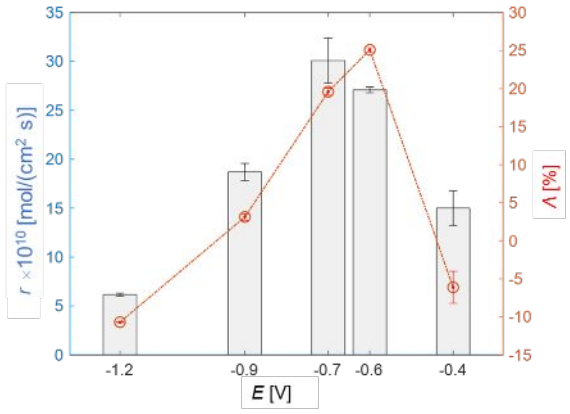

Fig. 7 Steady reaction rates (grey bar) and enhancement factors (red) at applied voltages of -0.4, -0.6, -0.7, -0.9, and -1.2 V. The error bars are standard deviations. Currents at different applied voltages are shown in Fig. 6 (b).

The effect of the potential on the NH_3 production rate was studied by varying the applied potential. As shown in Fig. 6, the reaction rate was accelerated at negative potentials, reaching steady reaction rates of 1.50×10^{-9}, 2.71×10^{-9}, 3.07×10^{-9}, 1.87×10^{-9}, and 6.15×10^{-10} mol/(s cm^2) at -0.4, -0.6, -0.7, -0.9, and -1.2 V, respectively. For the production rates at OCV, -0.4 V, -0.6 V, -0.7 V, -0.9 V, and -1.2 V, the transition response periods were 0–130 min (0–7800 s), 0–180 min (0–10800 s), 0–330 min (0–19800 s), 0–240 min (0–14400 s), 0–210 min (0–12600 s), and 0–60 min (0–3600 s), respectively. The steady states were reached after the transition response periods, and the steady reaction rates were measured over 120 min. The maximum steady NH_3 production rate was achieved at -0.7 V. At higher potentials, the reaction rate decreased significantly and even led to a negative Λ value at -1.2 V (Fig. 7), indicating that the catalytic activity at -1.2 V was lower than that at the OCV.

Model for the slow response and potential dependence of the NH_3 production rate

As no N_2H_4 was detected and the reactions were carried out under a mixed gas flow at a high temperature, the electrochemical nitrogen reduction reaction (NRR) was assumed to proceed via the dissociative pathway. The NRR via the dissociative pathway involves the following steps:

$$N_2 + 2* \xrightarrow{k_1} 2N* \qquad \#eq.1$$

$$N* + 3H_s \xrightarrow{k_2} * + NH_3 + 3V_H \qquad \#eq.2$$

$$H_2 + 2V_H \xrightarrow{k_3} 2H_s \qquad \#eq.3$$

$$\text{(Tafel)}\ 2H_s \xrightarrow{k_{-3}} H_2 + 2V_H \qquad \#eq.4$$

$$\text{(Volmer)}\ V_H + H^+ + e^- \xrightarrow{k_4} H_s \qquad \#eq.5$$

$$\text{(Heyrovsky)}\ H_s + H^+ + e^- \xrightarrow{k_5} H_2 + V_H \qquad \#eq.6$$

In these reaction steps, * is a N active site, V_H is a H active site, and N* and H_s are adsorbed N and H atoms, respectively. The reaction rate constants for each equation are represented as k_i (i = 1, 2, 3/-3, 4, 5). The hydrogen evolution reaction (HER) proceeds via the Volmer–Tafel mechanism (eqs. 4 and 5) and/or the Volmer–Heyrovsky mechanism (eqs. 5 and 6).[28] A previous density functional theory study on the HER on metal electrodes showed that the Volmer reaction is the fastest step, whereas the Tafel reaction is the rate-determining step. Furthermore, the rate of the Tafel reaction is indirectly influenced by the H coverage on the surface.[29] The NH_3 production rates as functions of reaction time at various applied potentials were fitted based on the above reaction equations. In addition, the

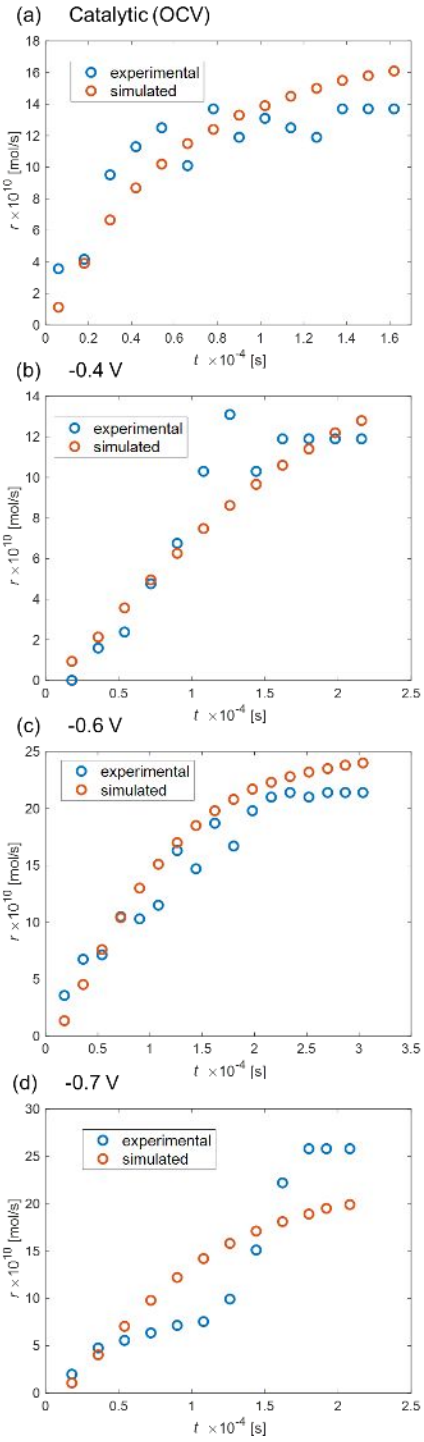

Fig. 8 Simulated (orange) and experimental (blue) NH_3 production rates under **(a)** catalytic conditions and at applied voltages of **(b)** -0.4 V, **(c)** -0.6 V, and **(d)** -0.7 V.

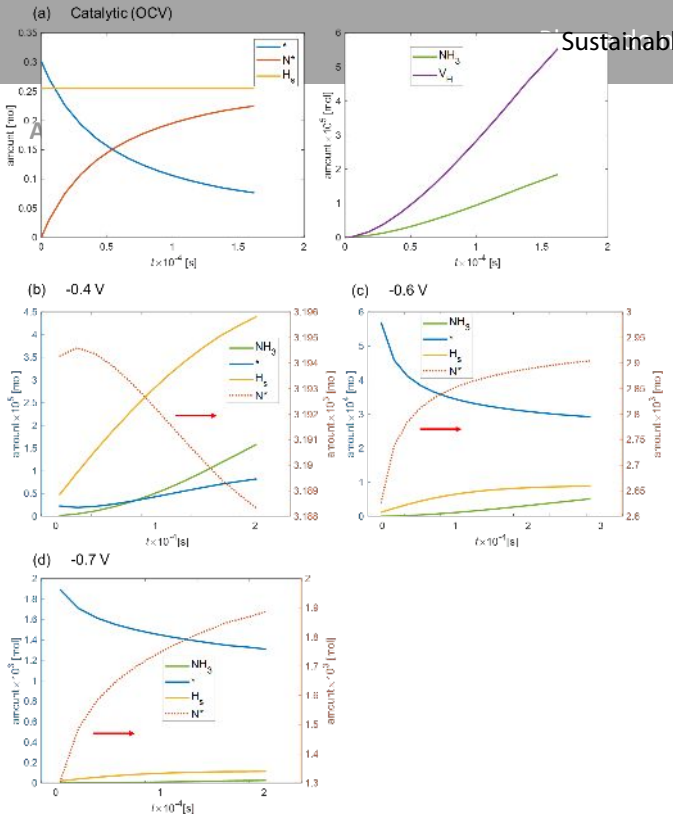

Fig. 9 Amounts of various species produced as a function of reaction time under **(a)** catalytic conditions and at applied voltages of **(b)** -0.4 V, **(c)** -0.6 V, and **(d)** -0.7 V. In (b)–(d), the amount of N* (dotted red line) corresponds to the right vertical axis.

following assumptions were included in the fitting model. (1) As the NH_3 generation reaction was initiated after the catalyst reduction pretreatment, the initial coverage of N active sites (*) is 0, whereas that of H active sites (V_H) is 1. (2) The k_i (i = 2, 3/-3, 4, 5) values are fitted as common parameters. (3) At the applied voltages, as the amount of protons (H^+) supplied is much higher than H_s used for NH_3 production, H_s is only generated by combining H^+ and e^-; thus, eq. 3 does not occur under an applied potential. (4) The catalytic NH_3 synthesis step (eq. 2) is much faster than the direct interaction of N*, H^+, and e^-; therefore, NH_3 production by $\mathrm{N*} + 3\mathrm{H}^+ + 3\mathrm{e}^- \rightarrow \mathrm{*} + \mathrm{NH_3}$ is ignored.[30] (5) For the catalytic reaction, only eqs. 1, 2, 3, and 4 were used in the simulation. As there was a continuous supply of excess reactants (H_2 and N_2), the concentrations of H_2 and N_2 in eqs. 1 and 3 were taken as dimensionless constants and defined as 1. To incorporate the effect of the concentration of H_S on the production rate, the reaction rate equation eq. 1 was given as:

$$2\frac{d\mathrm{N}*}{dt} = k_1[*]^2/[\mathrm{H_s}] \qquad \#eq.7$$

The experimental and simulated NH_3 production rates as functions of reaction time are plotted in Fig. 8. According to the simulation results, the slow production response under catalytic conditions and at applied voltages of -0.4, -0.6, and -0.7 V fitted well with the above model (Fig. 8). The obtained parameters and the amounts of each chemical species produced as a function of reaction time are shown in Table 1 and Fig. 9. The main NH_3 production reaction (eq. 2) and the Tafel step (eq. 4) were found to be almost independent of the applied voltage (Table 1). The reaction rate constant (k_2) for the main NH_3 production reaction (eq. 2) was 11.56 mol^{-3} s^{-1} under applied voltages and 2.74 mol^{-3} s^{-1} at the OCV. The reaction rate

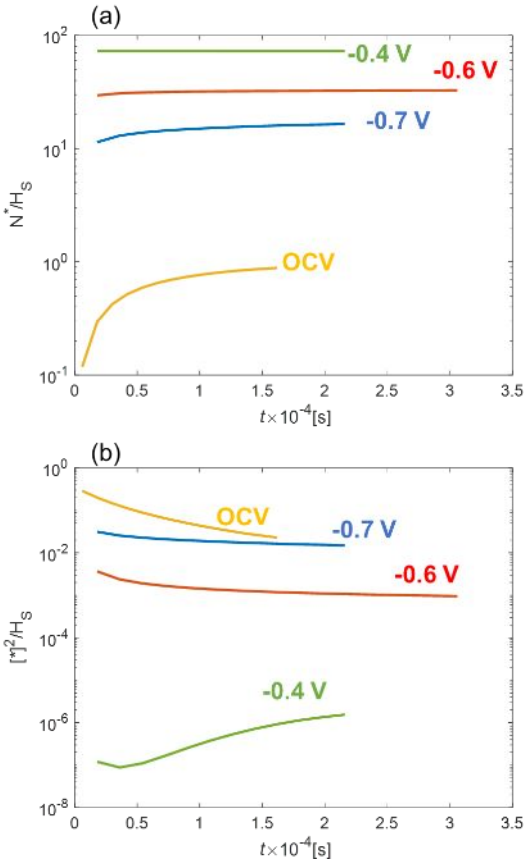

Fig. 10 (a) Ratio between adsorbed N (N*) and adsorbed H (H_S) as a function of reaction time. **(b)** [N active sites (*)]^2/H_S as a function of reaction time.

constant (k_{-3}) for the Tafel step (eq. 4) was 1.21 mol^{-1} s^{-1} under applied voltages and 1.28 mol^{-1} s^{-1} at the OCV. In contrast, the N_2 dissociation rate constant (k_1) varied significantly with the applied voltage. The value of k_1 at -0.4 V was approximately 4 times larger than that at the OCV (7.84 × 10^{-5} mol^{-1} s^{-1}), whereas those at -0.6 and -0.7 V were 1/40 and greater than 1/100 of the OCV value. Polarisation may lead to an Fe phase transition and consequently to a difference in k_1. Thus, the slow NH_3 production rate response may be due to not only the slow adsorption of N adatoms on the catalyst surface covered with H adatoms (Figs. 5 and 6) but also the slow formation of nitrides on the Fe surface during the NH_3 synthesis process,[31] as thus-formed nitrides can accelerate the NH_3 production rate. In addition, the Tafel step (eq. 4) is much faster than the Heyrovsky step (eq. 6). The reaction rate constant for N_2 dissociation (k_1) increased from the OCV to -0.4 V and then decreased as the applied voltage increased further. Both N* and H_s significantly decreased under applied voltages as compared to those under OCV conditions. However, H_s was reduced by a factor of 10,000, whereas N* was reduced by a factor of only 100, which could be the main factor responsible for the maximum NH_3 production rate being higher under applied voltages than in the OCV state. Therefore, the amount of N* being considerably greater than that of H_s is favourable for NH_3 production.

Figure 10 (a) shows N^*/H_S as a function of reaction time. Clearly, the amount of N* is much greater than that of H_S when a voltage is applied. Under the applied voltages, the maximum NH_3 production rate decreased in the order -0.7 V > -0.6 V > -0.4 V, which corresponds to the order in which N^*/H_S decreased as the applied voltage was changed from -0.7 to -0.4 V. Thus, although a higher N^*/H_S ratio is favourable for NH_3 formation, if the ratio is too high, NH_3 formation is hindered because few or no H atoms are adsorbed adjacent to N*. Figure 10 (b) shows $[*]^2/H_S$ as a function of reaction time. $[*]^2/H_S$ is related to the N_2 dissociation reaction rate equation (eq. 1), and the order of $[*]^2/H_S$ with respect to the applied voltage is the same as that of the NH_3 production rate from -0.7 to -0.4 V.

However, the above model resulted in large discrepancies between the experimental and calculated values at applied voltages of -0.9 and -1.2 V (the simulation plots are shown in Fig. S4). There are several possible explanations for such a discrepancy, especially at high applied voltages. Alternatively, excessive polarisation could destabilise the Fe-N phase, leading to a decreased rate of NH_3 production. Iron nitrides have a narrow range of compositions. In the Fe-N system, Fe_4N coexists with α-Fe up to 592 °C, with γ-Fe from 592 to 650 °C, and with ε-Fe below 680 °C. Fe_2N only coexists with ε-Fe up to approximately 500 °C.[24] As the N_2 dissociation rate constant could change with time during Fe phase transitions, the use of a constant value for the N_2 dissociation rate constant in the above model could result in fitting disparities.

Table 1 Parameters obtained by simulation

	OCV	-0.4 V	-0.6 V	-0.7 V
$k_1 \times 10^{-7}$ [$mol^{-1}s^{-1}$]	784	3170	20.6	4.71
k_2 [$mol^{-3}\ s^{-1}$]	2.74	11.56	11.56	11.56
$k_3 \times 10^5$ [$mol^{-1}\ s^{-1}$]	9.20	-	-	-
k_{-3} [$mol^{-1}\ s^{-1}$]	1.28	1.21	1.21	1.21
$k_4 \times 10^5$ [$s\ mol^{-2}$]	-	9.71	9.71	9.71
$k_5 \times 10^{-8}$ [$s\ mol^{-2}$]	-	6.54	6.54	6.54
* total amount $\times 10^{-3}$ [mol]	301	3.20	3.20	3.20
V_H total amount [mol]	0.255	557	557	557
N* steady state $\times 10^{-3}$ [mol]	225	3.19	2.91	1.91
H_s steady state $\times 10^{-5}$ [mol]	25500	4.40	8.92	11.5
N* coverage steady state	74.7%	99.7%	90.9%	59.7%
H_s coverage steady state	100%	7.90×10^{-6}%	1.60×10^{-5}%	2.06×10^{-5}%

Conclusions

In this work, an Fe-based catalyst with a BZY electrolyte, Fe/BZY, was used to synthesise NH_3 from N_2 and H_2 catalytically and electrochemically at ambient pressure and 500 °C. In the catalytic activity test, the steady NH_3 production rate was 2.10×10^{-9} mol/(g-cat s). However, electrochemical promotion was observed at applied voltages of -0.6, -0.7, and -0.9 V, with the maximum steady NH_3 production rate of 3.07×10^{-9} mol/(cm^2 s) obtained at -0.7 V and the maximum enhancement factor Λ of 25.1% achieved at -0.6 V. At highly negative applied voltages, Λ became negative. The observed electrochemical promotion of NH_3 production was explained by modelling the transient response of the NH_3 production rate to the polarisation. The fitting results suggested that under applied voltages, the amount of N* (adsorbed N atoms) on the electrode catalyst surface became considerably greater than the amount of H_s (adsorbed H atoms), which accelerated the NH_3 production rate. Furthermore, the NH_3 production rate response to applied voltages was slow, which could be due to a phase transition of Fe in Fe/BZY caused by polarisation. As the Fe/BZY catalyst tends to be oxidised at high temperatures in oxidative conditions, the electrocatalytic synthesis of NH_3 in a two-chamber reactor using steam and N_2 at ambient pressure will be the focus of future work.

Author Contributions

Yao Yuan: Conceptualization, Data curation, Formal analysis, Writing - original draft. **Shohei Tada:** Investigation, Resources. **Ryuji Kikuchi:** Conceptualization, Supervision, Writing - review & editing.

Conflicts of interest

The authors declare no conflicts of interest.

Acknowledgements

This work was supported by the Japan Society for the Promotion of Science (JSPS) KAKENHI grant 20H02521 and the Japan Science and Technology Agency (JST) CREST JPMJCR1441. Y.Y. was financially supported by the Graduate School of Engineering, The University of Tokyo Doctoral Student Special Incentives Program (SEUT). Y.Y. would like to thank Dr. Naoya Fujiwara for helpful comments and Mr. Ryuichi Ohori for discussions regarding the model.

Notes and references

1 Guo, C., Ran, J., Vasileff, A., and Qiao, S.-Z., Energy Environ. Sci., 11, 45-56 (2018).
2 Kugler, K., Ohs, B., Scholz, M., and Wessling, M., Phys. Chem. Chem. Phys., 16, 6129-6138 (2014).
3 Klerke, A., Christensen, C. H., Nørskov, J. K., and Vegge, T., J. Mater. Chem., 18, 2304-2310 (2008).
4 Kobayashi, H., Hayakawa, A., Somarathne, K. D. K. A., and Okafor, E. C., Proc. Combust. Inst., 37, 109-133 (2019).
5 Molouk, A. F. S., Okanishi, T., Muroyama, H., Matsui, T., and Eguchi, K., J. Electrochem. Soc., 162, F1268-F1274 (2015).
6 Barański, A., Kotarba, A., Łagan, J. M., Pattek-Janczyk, A., Pyrczak, E., and Reizer, A., Appl. Catal. A, 112, 13-36 (1994).
7 Kyriakou, V., Garagounis, I., Vasileiou, E., Vourros, A., and Stoukides, M., Catal. Today, 286, 2-13 (2017).
8 Amar, I. A., Lan, R., Petit, C. T. G., and Tao, S., J. Solid State Electrochem., 15, 1845 (2011).
9 Ouzounidou, M., Skodra, A., Kokkofitis, C., and Stoukides, M., Solid State Ionics, 178, 153-159 (2007).
10 Guo, Y., Liu, B., Yang, Q., Chen, C., Wang, W., and Ma, G., Electrochem. Commun., 11, 153-156 (2009).
11 Kosaka, F., Nakamura, T., and Otomo, J., J. Electrochem. Soc., 164, F1323-F1330 (2017).
12 Zhang, M., Xu, J., and Ma, G., J. Mater. Sci., 46, 4690-4694 (2011).
13 Yun, D. S., Joo, J. H., Yu, J. H., Yoon, H. C., Kim, J.-N., and Yoo, C.-Y., J. Power Sources, 284, 245-251 (2015).
14 Kosaka, F., Nakamura, T., Oikawa, A., Otomo, J., ACS Sustainable Chem. Eng., 5, 10439-10446 (2017).
15 E. Vasileiou, V. Kyriakou, I. Garagounis, A. Vourros, A. Manerbino, W. G. Coors and M. Stoukides, *Topics in Catalysis*, 2015, **58**, 1193-1201.
16 Babilo, P., and Haile, S. M., J. Am. Ceram. Soc., 88, 2362-2368 (2005).
17 Tong, J., Clark, D., Bernau, L., Sanders, M., and O'Hayre, R., J. Mater. Chem., 20, 6333-6341 (2010).
18 Han, D., Otani, Y., Noda, Y., Onishi, T., Majima, M., and Uda, T., RSC Adv., 6, 19288-19297 (2016).
19 Yuan, Y., Kikuchi, R., Takagaki, A., and Oyama, S. T., ECS Trans., 78, 451-459 (2017).
20 Andersen, S. Z., Čolić, V., Yang, S., Schwalbe, J. A., Nielander, A. C., McEnaney, J. M., Enemark-Rasmussen, K., Baker, J. G., Singh, A. R., Rohr, B. A., Statt, M. J., Blair, S. J., Mezzavilla, S., Kibsgaard, J., Vesborg, P. C. K., Cargnello, M., Bent, S. F., Jaramillo, T. F., Stephens, I. E. L., Nørskov, J. K., and Chorkendorff, I., Nature, 570, 504-508 (2019).
21 Greenlee, L. F., Renner, J. N., and Foster, S. L., ACS Catal., 8, 7820-7827 (2018).
22 Yuan, Y., Tada, S., and Kikuchi, R., Mater. Adv., 2, 793-803 (2021).
23 Ronduda, H., Zybert, M., Patkowski, W., Ostrowski, A., Jodłowski, P., Szymański, D., Kępiński L., and Raróg-Pilecka, W., RSC Adv., 11, 14218-14228 (2021).
24 Klotz, S., Le Godec, Y., Strässle, T., and Stuhr, U., Appl. Phys. Lett., 93, 091904 (2008).
25 Wriedt, H. A., Gokcen, N. A., and Nafziger, R. H., Bull. Alloy Phase Diagrams, 8, 355-377 (1987).
26 Yiokari, C. G., Pitselis, G. E., Polydoros, D. G., Katsaounis, A. D., and Vayenas, C. G., J. Phys. Chem. A, 104, 10600-10602 (2000).
27 Yentekakis, I. V., and Bebelis, S., J. Catal., 137, 278-283 (1992).
28 Tian, X., Zhao, P., and Sheng, W., Adv. Mater., 31, 1808066 (2019).
29 Skúlason, E., Tripkovic, V., Björketun, M. E., Gudmundsdóttir, S., Karlberg, G., Rossmeisl, J., Bligaard, T., Jónsson, H., and Nørskov, J. K., J. Phys. Chem. C, 114, 18182-18197 (2010).
30 C.-I. Li, H. Matsuo and J. Otomo, *RSC Advances*, 2021, **11**, 17891-17900.
31 Kandemir, T., Schuster, M. E., Senyshyn, A., Behrens, M., and Schlögl, R., Angew. Chem. Int. Ed., 52, 12723-12726 (2013).